Satellite Estimation of Aboveground Biomass and Impacts of Forest Stand Structure

Dengsheng Lu, Mateus Batistella, and Emilio Moran

Abstract

Heterogeneous Amazonian landscapes and complex forest stand structure often make aboveground biomass (AGB) estimation difficult. In this study, spectral mixture analysis was used to convert a Landsat Thematic Mapper (TM) image into green vegetation, shade, and soil fraction images. Entropy was used to analyze the complexity of forest stand structure and to examine impacts of different stand structures on TM reflectance data. The relationships between AGB and fraction images or TM spectral signatures were investigated based on successional and primary forests, respectively, and AGB estimation models were developed for both types of forests. Our findings indicate that the AGB estimation models using fraction images perform better for successional forest biomass estimation than using TM spectral signatures. However, both models based on TM spectral signatures and fractions provided poor performance for primary forest biomass estimation. The complex stand structure and associated canopy shadow greatly reduced relationships between AGB and TM reflectance or fraction images.

Introduction

The Brazilian Amazon basin has become one of the world's major contributors of carbon to the atmosphere due to its high deforestation rates in recent decades (Fearnside and Guimarães, 1996; Fearnside, 1999). Regional changes in biomass have been associated with important outcomes in ecosystem functional characteristics and climate change. Biomass determines potential carbon emissions that could be released to the atmosphere due to deforestation. Accurate biomass estimation is necessary to understand the impacts of deforestation on global change and environmental degradation. During the past decade, research focusing on tropical forest biomass estimation has attracted increasing attention (Overman *et al.*, 1994; Brown *et al.*, 1995; Nelson *et al.*, 1999; Ketterings *et al.*, 2001; Lu *et al.*, 2002a). However, biomass estimation over large areas in tropical regions is difficult using traditional field inventory methods. The advantages of remotely sensed data (e.g., multispectral and multitemporal images, a synoptic view, and a digital format allowing computer processing) have made it an important source for biomass estimation over large areas. In particular, Landsat Thematic Mapper (TM) (Nelson *et al.*, 1988; Sader *et al.*, 1989; Foody *et al.*, 1996; Roy and Ravan, 1996; Boyd *et al.*, 1999; Nelson *et al.*, 2000; Steininger, 2000; Lu *et al.*, 2002a; Foody *et al.*, 2003; Vieira *et al.*, 2003) and synthetic aperture radar (SAR) (Rignot *et al.*, 1995; Luckman *et al.*, 1997; Luckman *et al.*, 1998; Santos *et al.*, 2003) are the most often used data for biomass estimation, which is based on the statistical relationships between biomass and TM or SAR responses. Although various biomass estimation methods have been tested, rarely has research been successfully conducted for large areas in moist tropical regions. Previous research has shown the difficulty of estimating biomass based on TM spectral features because of the influence of increased canopy shadowing within large stands and the heterogeneity of vegetation stand structures (Roy and Ravan, 1996; Steininger, 2000; Lu, 2001).

Optical sensor data such as TM mainly capture mixed information over the vegetation cover: green leaves, canopy shadows, stems and branches, understory cover, and even soil beneath vegetation. Because of this complexity, changes of TM spectral features often do not directly reflect changes of biomass (Lu, 2001). This often leads to poor biomass estimation results based solely on TM spectral features. However, it may be possible to improve biomass estimation results by reducing the influences caused by canopy shadowing, stem and branch reflectance, and soil if different proportions of selected features can be identified within the mixed pixels. Linear spectral mixture analysis (LSMA) is often used to decompose the mixed pixel values into different proportions based on selected components (Roberts *et al.*, 1998; Shimabukuro *et al.*, 1998; Lu *et al.*, 2003) and has long been recognized as an effective method in handling spectral mixture problems. LSMA has been used to estimate different biophysical parameters, such as abundance in heterogeneous canopies (Gilabert *et al.*, 2000), leaf area index (Garcia-Haro *et al.*, 1996; North, 2002), and net primary productivity (Hall *et al.*, 1995; Peddle *et al.*, 1999; Peddle *et al.*, 2001). In this paper we evaluate the potential of biomass estimation using LSMA in the Brazilian Amazon basin and the effects of forest stand structure on TM reflectance and fractions.

Description of the Study Area

Rondônia has experienced high deforestation rates during the past two decades (INPE, 2002). Following the national

D. Lu and E. Moran are with the Center for the Study of Institutions, Population, and Environmental Change (CIPEC) Indiana University, 408 N Indiana Ave., Bloomington, IN (dlu@indiana.edu).

M. Batistella and E. Moran are with the Anthropological Center for Training and Research on Global Environmental Change (ACT), Indiana University, Bloomington, IN (moran@indiana.edu).

M. Batistella is with the Brazilian Agricultural Research Corporation, Embrapa Satellite Monitoring Campinas, São Paulo, Brazil. (mb@cnpm.embrapa.br).

Photogrammetric Engineering & Remote Sensing
Vol. 71, No. 8, August 2005, pp. 967–974.

0099-1112/05/7108–0967/$3.00/0

strategy of regional occupation and development, colonization projects initiated by the Brazilian government in the 1970s played a major role in this process (Moran, 1981). Most colonization projects in the state were designed to settle landless migrants. The immigrants transformed the forested landscape into a patchwork of cultivated crops, pastures, and different stages of successional forests. Over the Amazon region, 30 percent to 50 percent of the deforested area is in some stage of secondary succession (Moran *et al.*, 1994; Skole *et al.*, 1994; Lucas *et al.*, 2000; Roberts *et al.*, 2002; Ballester *et al.*, 2003), requiring that we carefully evaluate the biomass and carbon dynamics represented by their dynamic vegetation components.

The study area is located at Machadinho d'Oeste in northeastern Rondônia (Figure 1). Settlements were implemented in the mid-1980s in this study area, thus very limited deforestation occurred before 1988 as found on the 1988 TM image. However, deforestation rapidly increased in the 1990s and converted the primary forest into coffee plantation, agro-forestry, pasture, and successional forests. The majority of successional forests were less than 10 years old on the 1998 TM image, so the stand structure is significantly different between successional and primary forests in this study area. A detailed description of the characteristics of successional and primary forests is described in Lu *et al.* (2003).

In this study area, terrain is undulating, ranging from 100 m to 450 m above sea level. The primary tree communities are *Imbauba, Lacre, Leguminosae, Mimosoideae, Parapara*, and *Urucum*. Several soil types, mainly alfisols, oxisols, ultisols, and alluvial soils, were identified (Bognola and Soares, 1999). The climate is classified as equatorial hot and humid, with tropical transition. The well-defined dry season lasts from June to August, the annual average precipitation is 2,016 mm, and annual average temperature is 25.5° C (Rondônia, 1998).

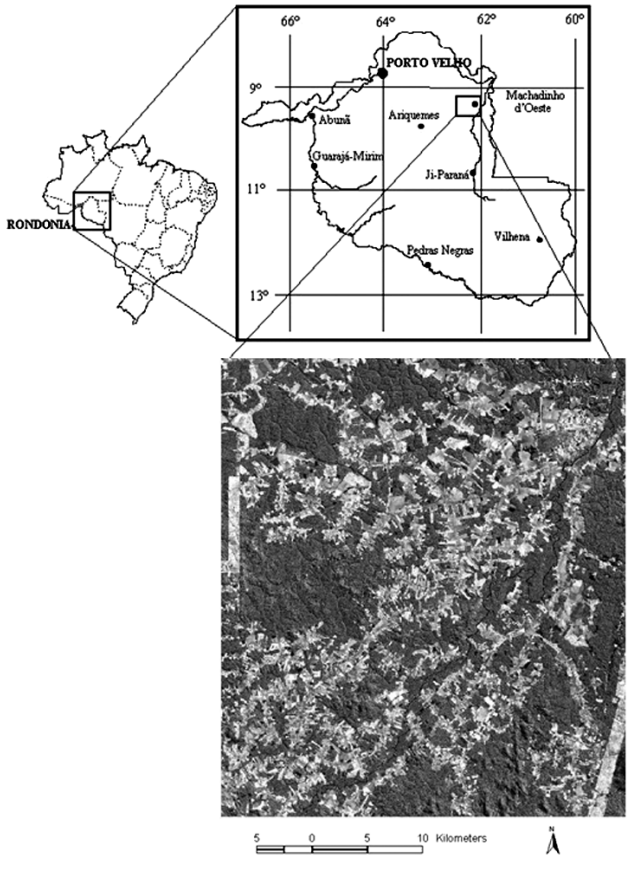

Figure 1. Location of Machadinho d'Oeste in the state of Rondônia, Brazil.

Methods

Field Data Collection and Biomass Calculation

Fieldwork was conducted in August 1999. The procedure used for surveying vegetation was a multilevel technique adapted from methods used at the Center for the Study of Institutions, Population, and Environmental Change (Ostrom, 1998). Preliminary image classification and band composite printouts indicated candidate areas to be surveyed, and a flight over the areas provided visual insights about the size, condition, and accessibility of each site. The surveys were conducted in areas with relatively homogeneous ecological conditions (i.e., topography, distance from water, and land use) and uniform physiognomic characteristics. After defining the area to be surveyed (plot sample), center points for three sets of nested subplots (1 m^2, 9 m^2, and 100 m^2) were randomly located to cover the variability within the plot sample (Lu *et al.*, 2004). Seedlings were defined as young trees or shrubs with a stem diameter smaller than 2 cm. Saplings were defined as young trees with a stem diameter at breast height (DBH) greater than 2 cm and smaller than 10 cm. Trees were defined as those woody plants with a DBH equal to or greater than 10 cm. Total tree height, stem height (the height of the first main branch), and DBH were measured for all trees in the three, 10 m × 10 m subplots within each plot. Height and DBH were measured for all saplings in the three nested 3 m × 3 m subplots. Ground-cover estimation and individual counting were carried out for seedlings and herbaceous vegetation in the three nested 1 m × 1 m sub-plots. The aboveground biomass was then aggregated at the plot level based on the measurements in nested subplots. Every plot was registered with a global positioning system to allow further integration with spatial data in geographic information systems and image processing systems. Forty sample plots were inventoried, including 26 plots for successional forests and 14 for primary forests. Table 1 summarizes the sample plot allocation

TABLE 1. SAMPLE PLOT DISTRIBUTION WITH BIOMASS DENSITY AND STATISTICAL CHARACTERISTICS OF THE SAMPLE DATA IN SUCCESSIONAL AND PRIMARY FORESTS IN RONDÔNIA, BRAZIL

		Successional Forest		Primary Forest	
		Range of Biomass Density (kg/m^2)	Number of Sample Plots	Range of Biomass Density (kg/m^2)	Number of Sample Plots
Plot distribution vs. range of biomass density		2–5	8	10–15	4
		5–8	4	15–20	2
		8–11	6	20–25	2
		11–14	5	25–30	2
		14–17	3	30–50	4
Total plots			26		14
Statistical information of biomass density	Mean		8.930		24.765
	Minimum		2.397		11.132
	Maximum		15.987		49.470
	Std. Dev.		4.349		11.805

with biomass distribution and statistical description of collected data for successional and primary forests.

Equation 1 was used to calculate individual tree biomass (Brown *et al.*, 1995), and Equation 2 was used to calculate individual sapling biomass (Honzák *et al.*, 1996):

$$YT = 0.0326 \times DT^2 \times H, \text{ and} \quad (1)$$

$$YS = \exp[-3.068 + 0.957 \times \ln(DS^2 \times H)], \quad (2)$$

where DT and DS are the tree and sapling DBH in centimeters, respectively; H is the total tree or sapling height in meters; and YT and YS are the biomasses in kilograms of individual trees and saplings, respectively. Aboveground biomass (AGB) in kg/m^2 is then calculated through Equation 3:

$$AGB = \sum_{i=1}^{m} YT_i/PA + \sum_{j=1}^{n} YS_j/SPA, \quad (3)$$

where m and n are the total number of trees and saplings, respectively, in the three nested subplots within one plot. PA and SPA are the total subplot areas (in m^2) in one plot for measuring trees (i.e., three 10 m $\times$ 10 m) and saplings (i.e., three 3 m $\times$ 3 m), respectively.

Analysis of Forest Stand Structure

Different tree parameters, such as tree height, DBH, crown size, etc. may be used to describe the characteristics of forest stand structure. In particular, the distribution of tree height is a good way to illustrate the vertical structure of a forest stand. In this research, entropy (*ENT*) was used to evaluate the complexity of a stand structure based on the probability of tree height distribution at the plot level. It can be expressed as

$$ENT = -\sum_{i=j}^{h} P_i \log_2(P_i) \text{ and } P_i = \frac{n_i}{\sum_{i=j}^{h} n_i}, \quad (4)$$

where P_i is the probability for i^{th} tree height, n_i is the number of trees in the i^{th} tree height, j is the minimum tree height, and h is the maximum tree height. For successional forest plots, j is equal to or greater than 5 m because the majority of trees have heights greater than 5 m. For primary forest, j is equal to or greater than 10 m, because the majority of trees have heights greater than 10 m. In general, higher complexity in the forest stand structure yields a higher *ENT* value.

In a forested area, an emergent has considerable influence on its neighboring vegetation and impacts remotely sensed observations due to its height and large crown and associated shade. Entropy can effectively reflect the complexity of forest stand structure, but cannot reflect the impacts from emergent. So to compensate the difference of maximum and minimum values of the tree height, the adjusted entropy (*ADJENT*) was defined as:

$$ADJENT = 0.1 * (h - j) * ENT. \quad (5)$$

A linkage of *ADJENT* data with relationships between AGB and TM spectral signatures or fraction images can be used to analyze how different stand structures affect vegetation reflectance and fraction composition, then further to analyze the impacts of the stand structures on AGB estimation.

The boxplot method was used to illustrate how biomass growth affects TM reflectance and fraction changes. A boxplot is a summary plot based on the median, quartiles, and extreme values. The box represents the inter-quartile range that contains 50 percent of the values. The *whiskers* are lines that extend from the box to the highest and lowest values, excluding outliers. A line across the box indicates the median. Five biomass groups for successional forests (i.e., 2–5, 5–8, 8–11, 11–14, and 14–17 kg/m^2) and for primary forests (10–15, 15–20, 20–25, 25–30, and 30–50 kg/m^2), respectively were analyzed. Three to eight sample plots for each successional forest group, and two to four plots for each primary forest group were aggregated.

TM Image Preprocessing

Accurate geometric rectification and atmospheric calibration are two important aspects in image preprocessing. In this research, TM data acquired on 18 June 1998 were geometrically rectified using control points taken from topographic maps at 1:100000 scale (Universal Transverse Mercator, South Zone 20). Nearest-neighbor re-sampling was used, and a root-mean-square error with less than 0.5 pixels was obtained. An improved image-based dark object subtraction model was used to implement atmospheric correction (Lu *et al.*, 2002b). The gain and offset for each band and sun elevation angle were obtained from the image header file, and the path radiance was identified based on clear water for each band. The atmospheric transmittance values for visible and near infrared bands were the averages for each spectral band derived from radiative transfer code (Chavez, 1996). For shortwave infrared bands, the atmospheric transmittance was set to 1. The surface reflectance values after calibration fell within the range of 0 to 1. For the convenience of data analysis, the reflectance values were rescaled to the range of 0 to 100 by multiplying 100 for each pixel.

Linear Spectral Mixture Analysis (LSMA)

LSMA is a physically based image processing method. It assumes that the spectrum measured by a sensor is a linear combination of the spectra of all pure materials (endmembers) within the pixel (Roberts *et al.*, 1998). The mathematic model of LSMA can be expressed as

$$R_i = \sum_{k=1}^{n} f_k R_{ik} + \varepsilon_i, \quad (6)$$

where i is the number of spectral bands used; $k = 1, \ldots,$ n (number of endmembers); R_i is the spectral reflectance of band i of a pixel that contains one or more endmembers; f_k is the proportion of endmember k within the pixel; R_{ik} is the known spectral reflectance of endmember k within the pixel on band i; and ε_i is the error for band i. A detailed description of the LSMA approach can be found in Roberts *et al.* (1998) and Mustard and Sunshine (1999).

Although much research for endmember selection has been explored (Bateson and Curtiss, 1996; Tompkins *et al.*, 1997; Roberts *et al.*, 1998; Mustard and Sunshine, 1999; Van der Meer, 1999; Dennison and Roberts, 2003), the image endmember is still the often used approach in many applications of LSMA because it can be obtained easily and represents spectra measured at the same scale as the data (Roberts *et al.*, 1998). The endmembers are often derived from the extremes of the image feature space, assuming they represent the purest pixels in the images (Mustard and Sunshine, 1999; Lu *et al.*, 2003). In this research, three image endmembers (shade, soil, and green vegetation (GV)) were identified from the scattergrams of TM3 and TM4 and of TM4 and TM5. A constrained least-squares solution was used to un-mix the TM image into three fraction images.

Integration of Image Data and Vegetation Inventory Data

A window size of 3 $\times$ 3 pixels was used to create an area of interest (AOI) for each plot using ERDAS Imagine® software.

Retrieval of mean value for each plot on TM reflectance or fraction images was conducted based on an overlay of the AOI layer on corresponding TM or fraction images. After the image values for these plots of successional and primary forests were extracted, Pearson's correlation coefficient was used to analyze relationships between AGB and image data, including TM spectral and fraction data. Because the correlation coefficient measures the strength of linear relationships between two variables (Runyon *et al.*, 2000), the analysis of correlation coefficients provides a way to find potential variables for developing AGB estimation models. The AGB was used as a dependent variable, TM spectral bands or fraction images were used as independent variables, and a stepwise regression analysis was used to develop AGB estimation models for successional and primary forests. The coefficient of determination (R^2) is used to evaluate a regression model performance because it measures the percent of variation explained by the regression model.

Results and Discussion

Impacts of Forest Stand Structure on Biomass Estimation

Vegetation stand structure and associated canopy shadows, canopy closure, and species composition were regarded as important factors affecting the vegetation reflectance captured by optical sensors (Steininger, 2000; Lu, 2001). Figure 2 graphically illustrates the relationships between TM spectral signatures and AGB. Bands 1, 2, and 3 are not shown in Figure 2 because they often have relatively weak correlations with AGB (Lu, 2001). For successional forests, vegetation reflectance in shortwave infrared bands (TM5 and TM7) decreases slightly as AGB increases, but such decrease in near infrared band (TM4) is obvious. For primary forest, the relationship between reflectance and AGB is not obvious, although AGB varies greatly from approximately 11 kg/m^2 to 50 kg/m^2. This implies that the reflectance of primary forest is saturated due to its complex stand structure.

Figure 3 graphically illustrates the relationships of the GV and shade fractions with AGB. The soil and error fractions are not shown in this graph because of their weak correlations with AGB and very small values for successional and primary forests. For successional forests, GV fraction obviously decreases but shade fraction increases as AGB increases. In primary forest, the relationship of shade or GV fraction with AGB is not as obvious as biomass increases.

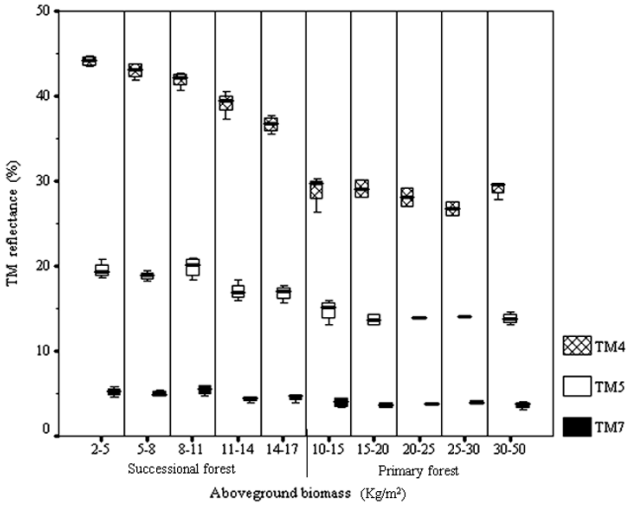

Figure 2. Comparison of relationships between aboveground biomass and TM reflectance values (bands TM4, TM5, and TM7) of successional and primary forests.

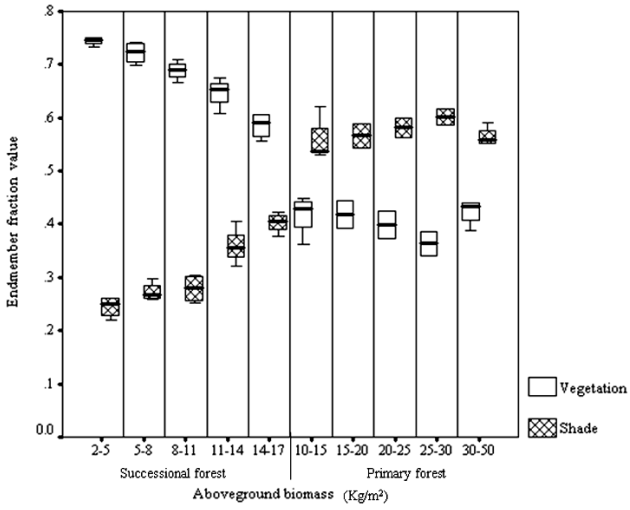

Figure 3. Comparison of relationships between aboveground biomass and endmember fractions (green vegetation and shade fractions) of successional and primary forests.

An obvious feature in Figures 2 and 3 is the gap in reflectance (especially band 4) and fraction values between successional and primary forests. Such a situation was caused by the sample data collected in this study area. The different vegetation stand structures between successional and primary forests (Lu *et al.*, 2003) lead to an abrupt change in the spectral signatures or fraction values between them. However, the trends of differences in TM reflectance or fraction values between successional and primary forests implies that these gaps would decrease or disappear as successional forests grow to more mature stages. Another obvious feature is a small peak in TM5 when AGB falls in the 8–11 kg/m^2 group in successional forests and a small trough in TM4 in primary forest when AGB falls in the 25–30 kg/m^2 group (see Figure 2). A similar situation occurs in shade fraction in successional forests and in shade and GV fractions in primary forest (see Figure 3).

The stand structures in primary forest are more complex than in successional forests, particularly for those sites with large AGB amounts. In initial succession, seedlings and saplings account for most of the AGB amount. The lack of stratification and a structured canopy of trees results in high GV but low shade fraction values. In advanced succession, trees occupy the canopy with obvious stratification of multilayer structures. This feature results in significantly reduced GV fraction but increased shade fraction compared with initial succession. In primary forest, the majority of the AGB is in woody vegetation, and a well-stratified and well-structured vegetation stand is formed. This makes a lower GV fraction but higher shade fraction than successional forests. In those sites with large AGB, the higher canopy shadow caused by emergents is one of the main factors resulting in data saturation, particularly in primary forests.

Table 2 illustrates the complexity of forest stand structure for selected plots. In general, the forest stand structure

TABLE 2. COMPARISON OF VEGETATION STAND STRUCTURES AMONG THE SELECTED SAMPLE PLOTS

Forest Type	Plot_ID	Biomass Density (kg/m^2)	Tree Height Range (m)	Number of Trees	ENT	Diff. of Range (m)	ADJENT	Biomass Range (kg/m^2)
Successional Forests	RO-08	2.965	5–6	1	0	1	0	2–5
	RO-10	3.397	9–11	2	1.000	2	0.200	
	RO-03	3.597	6–11	16	1.592	5	0.796	
	RO-21	3.891	6–11	13	1.296	5	0.648	
	RO-19	3.909	5–11	16	2.125	6	1.275	
	RO-16	4.297	6–11	9	2.059	5	1.030	
	RO-23	4.644	7–15	16	2.578	8	2.062	
	RO-07	4.947	8–13	19	2.104	5	1.052	
	RO-28	6.418	6–14	16	2.750	8	2.200	5–8
	RO-05	7.695	7–14	20	2.526	7	1.768	
	RO-43	7.700	6–16	19	3.076	10	3.076	
	RO-26	7.910	8–16	18	2.642	8	2.114	
	RO-20	8.505	7–16	23	2.703	9	2.433	8–11
	RO-15	8.538	7–13	34	2.131	6	1.279	
	RO-31	8.956	8–17	30	2.376	9	2.138	
	RO-37	9.259	7–16	27	2.712	9	2.441	
	RO-11	9.297	7–13	24	2.422	6	1.453	
	RO-38	10.578	6–16	28	3.101	10	3.101	
	RO-24	12.364	7–17	18	2.858	10	2.858	11–14
	RO-02	12.510	9–19	27	2.980	10	2.980	
	RO-12	12.763	5–20	16	2.899	15	4.349	
	RO-13	12.771	9–18	24	2.834	9	2.551	
	RO-25	12.804	5–18	33	3.279	13	4.263	
	RO-06	14.812	6–18	21	2.887	12	3.464	14–17
	RO-04	14.963	9–22	40	3.485	13	4.531	
	RO-32	15.610	7–23	39	3.099	16	4.958	
Primary Forests	RO-36	11.132	10–18	10	2.722	8	2.178	10–15
	RO-42	12.500	10–18	16	2.656	8	2.125	
	RO-40	12.677	10–26	11	3.278	16	5.245	
	RO-33	13.401	10–17	13	2.412	7	1.688	
	RO-34	17.500	10–20	21	3.006	10	3.006	15–20
	RO-14	19.263	10–22	18	2.933	12	3.520	
	RO-01	21.027	10–24	27	3.288	14	4.603	20–25
	RO-09	24.370	11–25	21	3.237	14	4.532	
	RO-41	26.542	10–27	18	3.110	17	5.287	25–30
	RO-35	28.863	10–29	17	3.058	19	5.810	
	RO-30	32.871	11–31	14	2.692	20	5.384	30–50
	RO-39	34.843	10–32	17	3.007	22	6.615	
	RO-27	42.244	10–21	49	3.092	11	3.401	
	RO-17	49.170	11–26	19	3.195	15	4.793	

becomes more complex as AGB increases. The important influence of emergents on the complexity of stand structure is obvious. For example, the emergents in sample plots RO-12, RO-25, RO-04, and RO-32 in the successional forest category and RO-41, RO-35, and RO-39 in the primary forest category create more complex stand structure and associated canopy shades than others. Linkage of the *ADJENT* values and corresponding relationships between AGB and TM spectral signatures or fraction images can effectively explain the peaks and troughs that appear in Figures 2 and 3. For example, in successional forests, there are six sample plots in the 8–11 kg/m^2 group, but two of the plots have obviously simpler stand structures compared to the neighboring groups (the *ADJENT* values for RO–15 and RO–11 plots are less than 1.46). The relatively simple stand structure leads to a higher reflectance in TM5 and lower shade fraction than normal because of less impact from canopy shadows. In contrast, the complex stand structure of primary forest in the two sample plots falling in the 25–30 kg/m^2 group (the *ADJENT* values for RO-41 and RO-35 plots are greater than 5.2) yield lower reflectance in TM4 and higher shade but lower GV fractions than in neighboring groups (i.e., 20–25 and 30–50 kg/m^2 groups in Figures 2 and 3, respectively). The canopy shade increases when canopies become more heterogeneous with increasing numbers of gaps and emergents. The presence of gaps and emergents accounts for increasing shade, leading to higher shade fraction but lower GV fraction. Primary forests in different sites have highly variable AGB amounts depending on the soil condition, topography, and degradation by selective logging or fire. However, complex vegetation stand structures in primary forest and in advanced successional forests often result in similar TM reflectance even if AGB varies significantly. A similar situation is also found in other study areas such as in Manaus and Altamira of the Brazilian Amazon, where canopy reflectance of the successional forests saturated when biomass density increased to about 15 kg/m^2 or vegetation ages reached over 15 years (Steininger, 2000; Lu, 2001). However, different soil conditions and land-use history significantly affect the vegetation growth, resulting in significantly different stand structures even if their vegetation ages are similar (Moran *et al.*, 2000). For example, the poor soil condition and long-term land use history in Bragantina make the vegetation growth rate much lower than in other study areas such as Altmaira, resulting in much simpler stand structure and species composition (Lu, 2001). In this situation, 70-year-old successional forests still can be separated from primary forest based on TM spectral signatures (Vieira *et al.*, 2003). The biomass density of 70-year-old successional forests in Bragantina is only approximately 14 kg/m^2 (Vieira *et al.*, 2003), while in Altamira the biomass density can be 20 kg/m^2 for 15 year old (Lu et al., 2002a)

and in this study area it can be 15 kg/m^2 for 12 year old forests.

Relationships Between Biomass and Fraction Images and TM Spectral Signatures

Table 3 provides the correlation coefficients between fractions and AGB. For comparison, the correlations between TM spectral signatures and AGB are also provided in this table. For successional forests, GV fraction is strongly negatively correlated with AGB (−0.89), but the shade fraction is strongly positively correlated (0.88). The GV and shade relationships with AGB are slightly stronger than the relationships between TM spectral signatures and AGB (the highest coefficient between AGB and band TM4 is −0.86). However, the soil fraction is weakly correlated with successional forest AGB (−0.03). For primary forest, the GV and shade fractions are very weakly correlated with AGB. A similar situation for TM data is that no TM bands are significantly correlated with primary forest biomass. In contrast, the soil fraction has a stronger relationship with AGB than with GV and shade fractions. The shortwave infrared bands (TM5 and TM7) have stronger relationship with AGB than visible and near infrared bands. The strong relationships between successional forest biomass and GV or shade fraction implies that GV or shade fraction is suitable for successional forest biomass estimation, but the weak relationship between primary forest biomass and fractions imply that they may be not suitable for primary forest biomass estimation. A similar conclusion is that TM spectral signatures, especially the band TM4 in this study, may be suitable for successional forest biomass estimation but no spectral bands are suitable for primary forest biomass estimation.

Checking the relationships between primary forest biomass and soil (−0.425) or error fraction (−0.445) indicated that three endmembers (GV, shade, and soil) may be insufficient to un-mix the mixed pixels of primary forest into proportions of the different endmembers. Because of the complexity of forest stand structures in primary forest and impacts of sun elevation angle, the optical sensors may capture some information of non-photosynthetic vegetation (NPV), such as tree stems and branches. This information was mixed in soil and error fractions when only three endmembers were used (Roberts *et al.*, 1998). Hence, stratification of successional and primary forests may be an alternative to improve the quality of fraction images for the primary forests. The NPV, GV, and shade endmembers may be more suitable than GV, shade, and soil endmembers for unmixing primary forest. Some previous research used four endmembers (NPV, GV, soil, and shade, selecting from a combination of reference and image endmembers) in the LSMA approach in tropical forests (Roberts *et al.*, 1998) and has shown to be valuable for land-cover classification. Using reference endmembers based on field reflectance measurements has the potential to provide better fraction results than using image-based endmembers (Roberts *et al.*, 1998). However, selecting an NPV endmember based on the image itself is often difficult. Also, nonlinear spectral mixture analysis may be more appropriate in vegetation studies because significant multiple scattering of photons occurs in the vegetation (Ray and Murray, 1996). However, nonlinear mixture models are often difficult to build and convert (Gong and Zhang, 1999), and more research will be necessary in the future.

TABLE 3. CORRELATION COEFFICIENTS BETWEEN AGB AND FRACTIONS OR TM REFLECTANCE FOR SUCCESSIONAL FORESTS (SF) AND PRIMARY FOREST (PF)

Fractions			Spectral Signatures		
Fraction	SF	PF	TM	SF	PF
Soil	−0.033	−0.425	TM 1	−0.163	0.057
GV	−0.886[a]	0.075	TM 2	−0.550[b]	0.015
Shade	0.879[a]	0.088	TM 3	−0.455[b]	0.040
Error	0.134	−0.445	TM 4	−0.864[a]	0.032
			TM 5	−0.695[a]	−0.397
			TM 7	−0.515[b]	−0.287

[a]Correlation is significant at the 0.01 level.
[b]Correlation is significant at the 0.05 level.

Aboveground Biomass Estimation

AGB estimation models were developed based on the integration of sampled data from the field measurements and retrieved image values. Table 4 summarizes the best regression models for the successional and primary forests, based on TM bands and fraction images. The stepwise regression analysis of TM spectral bands and fraction images indicated that two or more TM images or fraction images can not significantly improve the regression performance. This is because strong correlations exist between some TM spectral bands used (e.g., bands TM2 and TM3) and between fraction images (e.g., strongly negative correlation between GV and shade fractions) or because weak relationships exist between AGB and some image data (e.g., between AGB and TM1, or between AGB and soil fraction).

For successional forests, the regression model using the GV fraction slightly improved estimation performance (i.e., 0.785) compared with using TM spectral band (0.746). The transformation of the GV fraction, i.e., GV/(1-GV), further increased the regression coefficient (from 0.785 to 0.812). For primary forest, neither fractions nor spectral signatures can provide good model performance for biomass estimation.

Our analysis indicates that using Landsat TM image is more successful for biomass estimation in successional forests than in primary forests. The complexity of forest stand structure in primary forest is the main factor making the biomass estimation difficult. Different soil conditions and topography can significantly influence vegetation growth and biomass accumulation rates (Moran *et al.*, 2000; Lu *et al.*, 2002c). In order to improve primary forest biomass estimation, some possible approaches (development of NPV fraction using LSMA, a combination of spectral and textures, incorporation of optical and SAR L-band or lidar data, and use of multi-source data such as spectral, texture, and ancillary) may improve the biomass estimation performance (Lu, 2001). Also, use of neural network for biomass estimation may provide better results than regression-based approaches (Foody *et al.*, 2003). More research is needed for primary forest biomass estimation.

TABLE 4. COMPARISON OF REGRESSION MODELS USING TM SPECTRAL AND FRACTION IMAGES FOR SUCCESSIONAL FORESTS (SF) AND PRIMARY FOREST (PF)

Type	Variable	Regression Models	R^2
SF	Fraction	Biomass = 48.674 − 57.904 · GV	0.785
		Biomass = 23.787 − 6.47 · GV/(1-GV)	0.812
	Spectral	Biomass = 66.772 − 1.392 · TM4	0.746
		Ln(biomass) = 7.853 − 0.14 · TM4	0.697
PF	Fraction	Biomass = 33.284 − 414.143 · Soil fraction	0.181
		Ln(biomass) = 3.386 − 13.688 · Soil fraction	0.120
	Spectral	Biomass = 102.414 − 5.496 · TM5	0.158
		Ln(biomass) = 6.626 − 0.249 · TM5	0.198

Note: Ln(biomass) = the natural logarithm of biomass; GV = green vegetation fraction; R^2 = coefficient of determination.

Conclusions

This paper explored the relationships between AGB and TM reflectance and between AGB and fractions and compared their biomass estimation performances. Our findings indicate that band TM4 and GV fraction are the most suitable of the variables tested for successional forest biomass estimation. Using the GV-based regression model improved the biomass estimation performance for the successional forest. However, neither TM reflectance nor fractions is suitable for primary forest biomass estimation. Canopy shadow and complex biophysical characteristics degrade AGB estimation performance using TM data. The *ADJENT* values indicated important impacts of complex forest stand structures on TM data, so methods to reduce the impacts of stand structures will be an important aspect to improve biomass estimation performance.

Acknowledgments

The authors wish to thank the National Science Foundation (Grants 95-21918 and 99-06826) and the National Aeronautics and Space Administration (Grant N005-334) for their support, which provided funds for the research.

References

Ballester, M.V.R., D de C. Victoria, A.V. Krusche, R. Coburn, R.L. Victoria, J.E. Richey, M.G. Logsdon, E. Mayorga, and E. Matricardi, 2003. A remote sensing/GIS-based physical template to understand the biogeochemistry of the Ji-Parana river basin (Western Amazonia), *Remote Sensing of Environment*, 87:429–445.

Bateson, A., and B. Curtiss, 1996. A method for manual endmember selection and spectral unmixing, *Remote Sensing of Environment*, 55:229–243.

Bognola, I.A., and A.F. Soares, 1999. *Solos das "glebas 01, 02, 03 e 06" do Município de Machadinho d'Oeste, RO. Pesquisa em Andamento*, n.10. Embrapa Monitoramento por Satélite, Campinas, Brazil, 7 p.

Boyd, D.S., G.M. Foody, and P.J. Curran, 1999. The relationship between the biomass of Cameroonian tropical forests and radiation reflected in middle infrared wavelengths (3.0–5.0 μm), *International Journal of Remote Sensing*, 20:1017–1023.

Brown, I.F., L.A. Martinelli, W.W. Thomas, M.Z. Moreira, C.A. cid Ferreira, and R.A. Victoria, 1995. Uncertainty in the biomass of Amazonian forests: an example from Rondônia, Brazil, *Forest Ecology and Management*, 75:175–189.

Chavez, P.S. Jr., 1996. Image-based atmospheric corrections – revisited and improved, *Photogrammetric Engineering & Remote Sensing*, 62:1025–1036.

Dennison, P.E., and D.A. Roberts, 2003. Endmember selection for multiple endmember spectral mixture analysis using endmember average RMSE, *Remote Sensing of Environment*, 87:123–135.

Fearnside, P.M., 1999. Forests and global warming mitigation in Brazil: opportunities in the Brazilian forest sector for responses to global warming under the "clean development mechanism," *Biomass and Bioenergy*, 16:171–189.

Fearnside, P.M., and W.M. Guimarães, 1996. Carbon uptake by secondary forests in Brazilian Amazonia, *Forest Ecology and Management*, 80:35–46.

Foody, G.M., G. Palubinskas, R.M. Lucas, P.J. Curran, and M. Honzák, 1996. Identifying terrestrial carbon sinks: classification of successional stages in regenerating tropical forest from Landsat TM data, *Remote Sensing of Environment*, 55:205–216.

Foody, G.M., D.S. Boyd, and M.E.J. Cutler, 2003. Predictive relations of tropical forest biomass from Landsat TM data and their transferability between regions, *Remote Sensing of Environment*, 85:463–474.

Garcia-Haro, F.J., M.A. Gilabert, and J. Melia, 1996. Linear spectral mixture modeling to estimate vegetation amount from optical spectral data, *International Journal of Remote Sensing*, 17:3373–3400.

Gilabert, M.A., F.J. Garcia-Haro, and J. Melia, 2000. A mixture modeling approach to estimate vegetation parameters for heterogeneous canopies in remote sensing, *Remote Sensing of Environment*, 72:328–345.

Gong, P., and A. Zhang, 1999. Noise effect on linear spectral unmixing, *Geographic Information Sciences*, 5:52–57.

Hall, F.G., Y.E. Shimabukuro, and K.F. Huemmrich, 1995. Remote sensing of forest biophysical structure using mixture decomposition and geometric reflectance models, *Ecological Applications*, 5:993–1013.

Honzák, M., R.M. Lucas, I. do Amaral, P.J. Curran, G.M. Foody, and S. Amaral, 1996. Estimation of the leaf area index and total biomass of tropical regenerating forests: a comparison of methodologies, *Amazonian Deforestation and Climate* (J.H.C. Gash, C.A. Nobre, J.M. Roberts, and R.C. Victoria, editors), John Wiley and Sons, Chichester, U.K., pp. 365–381.

Instituto Nacional de Pesquisas Espaciais (INPE), 2002. *Monitoring of the Brazilian Amazon Forest by Satellite 2000–2001*, INPE, São José dos Campos, SP, Brazil, 23 p.

Ketterings, Q.M., R. Coe, M. van Noordwijk, K. Ambagau, and C.A. Palm, 2001. Reducing uncertainty in the use of allometric biomass equations for predicting aboveground tree biomass in mixed secondary forests, *Forest Ecology and Management*, 146:199–209.

Lu, D. 2001. *Estimation of Forest Stand Parameters and Application in Classification and Change Detection of Forest Cover Types in the Brazilian Amazon Basin*, Ph.D. dissertation, Indiana State University, Terre Haute, Indiana, 235 p.

Lu, D., P. Mausel, E. Brondízio, and E. Moran, 2002a. Aboveground biomass estimation of successional and mature forests using TM images in the Amazon basin, *Advances in Spatial Data Handling* (D. Richardson and P. van Oosterom, editors), Springer-Verlag, New York, New York, pp. 183–196.

Lu, D., P. Mausel, E. Brondízio, and E. Moran, 2002b. Assessment of atmospheric correction methods for Landsat TM data applicable to Amazon basin LBA research, *International Journal of Remote Sensing*, 23:2651–2671.

Lu, D., E. Moran, and P. Mausel, 2002c. Linking Amazonian secondary succession forest growth to soil properties, *Land Degradation and Development*, 13:331–343.

Lu, D., E. Moran, and M. Batistella, 2003. Linear mixture model applied to Amazonian vegetation classification, *Remote Sensing of Environment*, 87:456–469.

Lu, D., P. Mausel, M. Batistella, and E. Moran, 2004. Comparison of Land-Cover Classification Methods in the Brazilian Amazon Basin, *Photogrammetric Engineering & Remote Sensing*, 70:723–731.

Lucas, R.M., M. Honzák, P.J. Curran, G.M. Foody, R. Milne, T. Brown, and S. Amaral, 2000. Mapping the regional extent of tropical forest regeneration stages in the Brazilian Legal Amazon using NOAA AVHRR data, *International Journal of Remote Sensing*, 21:2855–2881.

Luckman, A., J.R. Baker, T.M. Kuplich, C.C.F. Yanasse, and A.C. Frery, 1997. A study of the relationship between radar backscatter and regenerating forest biomass for space borne SAR instrument, *Remote Sensing of Environment*, 60:1–13.

Luckman, A., J. R.Baker, M. Honzák, and R.M. Lucas, 1998. Tropical forest biomass density estimation using JERS-1 SAR: seasonal variation, confidence limits, and application to image mosaics, *Remote Sensing of Environment*, 63:126–139.

Moran, E.F., 1981. *Developing the Amazon*, Indiana University Press, Bloomington, Indiana, 292 p.

Moran, E.F., E.S. Brondízio, P. Mausel, and Y. Wu, 1994. Integrating Amazonian vegetation, land use and satellite data, *BioScience*, 44:329–338.

Moran, E.F., E.S. Brondízio, J.M. Tucker, M.C. da Silva-Forsberg, S.D. McCracken, and I. Falesi, 2000. Effects of soil fertility and land use on forest succession in Amazonia, *Forest Ecology and Management*, 139:93–108.

Mustard, J.F., and J.M. Sunshine, 1999. Spectral analysis for earth science: investigations using remote sensing data, *Remote Sensing for the Earth Sciences: Manual of Remote Sensing*

(A.N. Rencz, editor), John Wiley and Sons, Inc., New York, New York, pp. 251–307.

Nelson, B.W., R. Mesquita, J.L.G. Pereira, S.G.A. de Souza, G.T. Batista, and L.B. Couto, 1999. Allometric regression for improved estimate of secondary forest biomass in the central Amazon, *Forest Ecology and Management*, 117:149–167.

Nelson, R., D.S. Kimes, W.A. Salas, and M. Routhier, 2000. Secondary forest age and tropical forest biomass estimation using Thematic Mapper imagery, *Bioscience*, 50:419–431.

Nelson, R., W. Krabill, and J. Tonelli, 1988. Estimating forest biomass and volume using airborne laser data, *Remote Sensing of Environment*, 24:247–267.

North, P.R.J., 2002. Estimation of f_{apar}, LAI, and vegetation fractional cover from ATSR-2 imagery, *Remote Sensing of Environment*, 80:141–121.

Ostrom, E. 1998. The international forestry resources and institutions research program: a methodology for relating human incentives and actions on forest cover and biodiversity, *Forest Biodiversity in North, Central, and South America and the Caribbean: Research and Monitoring* (F. Dallmeier and J.A. Comiskey, editors), Paris/New York: UNESCO/Parthenon, Vol. 21, pp. 1–28.

Overman, J.P.M., H.J.L. Witte, and J.G. Saldarriaga, 1994. Evaluation of regression models for aboveground biomass determination in Amazon rainforest, *Journal of Tropical Ecology*, 10:207–218.

Peddle, D.R., S.P. Brunke, and F.G. Hall, 2001. A comparison of spectral mixture analysis and ten vegetation indices for estimating boreal forest biophysical information from airborne data, *Canadian Journal of Remote Sensing*, 27:627–635.

Peddle, D.R., F.G. Hall, and E.F. LeDrew, 1999. Spectral mixture analysis and geometric-optical reflectance modeling of boreal forest biophysical structure, *Remote Sensing of Environment*, 67:288–297.

Ray, T.W., and B.C. Murray, 1996. Nonlinear spectral mixing in dissert vegetation, *Remote Sensing of Environment*, 55:59–64.

Rignot, E.J., R. Zimmerman, and J.J. van Zyl, 1995. Spaceborne applications of P band imaging radars for measuring forest biomass, *IEEE Transactions on Geoscience and Remote Sensing*, 33:1162–1169.

Roberts, D.A., G.T. Batista, J.L.G. Pereira, E.K. Waller, and B.W. Nelson, 1998. Change identification using multitemporal spectral mixture analysis: applications in eastern Amazônia, *Remote Sensing Change Detection: Environmental Monitoring Methods and Applications* (R.S. Lunetta and C.D. Elvidge, editors), Ann Arbor Press, Chelsea, Michigan, pp. 137–161.

Roberts, D.A., I. Numata, K. Holmes, G. Batista, T. Krug, A. Monteiro, B. Powell, and O.A. Chadwick, 2002. Large area mapping of land-cover change in Rondonia using decision tree classifiers, *Journal of Geophysical Research*, 107 (D20), 8073 LBA 40–1 to 40–18.

Rondônia, 1998. *Diagnóstico sócio-econômico do Estado de Rondônia e assistência técnica para formulação da segunda aproximação do zoneamento sócio-econômico-ecológico – Climatologia*, v. 1. Governo de Rondônia/PLANAFLORO, Porto Velho, Brazil, 401 p.

Roy, P.S., and S.A. Ravan, 1996. Biomass estimation using satellite remote sensing data – an investigation on possible approaches for natural forest, *Journal of Bioscience*, 21:535–561.

Runyon, R.P., K.A. Coleman, and D.J. Pettenger, 2000. *Fundamentals of Behavioral Statistics* (9th Edition), McGraw-Hill Higher Education, Boston, Massachusetts, 656 p.

Sader, S.A., R.B. Waide, W.T. Lawrence, and A.T. Joyce, 1989. Tropical forest biomass and successional age class relationships to a vegetation index derived from Landsat TM data, *Remote Sensing of Environment*, 28:143–156.

Santos, J.R., C.C. Freitas, L.S. Araujo, L.V. Dutra, J.C. Mura, F.F. Gama, L.S. Soler, and S.J.S. Sant' Anna, 2003. Airborne P-band SAR applied to the aboveground biomass studies in the Brazilian tropical rainforest, *Remote Sensing of Environment*, 87:482–493.

Shimabukuro, Y.E., G.T. Batista, E.M.K. Melio, J.C. Moreira, and V. Duarte, 1998. Using shade fraction image segmentation to evaluate deforestation in Landsat Thematic Mapper images of the Amazon region, *International Journal of Remote Sensing*, 19:535–541.

Skole, D.L., W.H. Chomentowski, W.A. Salas, and A.D. Nobre, 1994. Physical and human dimension of deforestation in Amazonia, *BioScience*, 44:314–328.

Steininger, M.K., 2000. Satellite estimation of tropical secondary forest aboveground biomass data from Brazil and Bolivia, *International Journal of Remote Sensing*, 21:1139–1157.

Tompkins, S., J.F. Mustard, C.M. Pieters, and D.W. Forsyth, 1997. Optimization of endmembers for spectral mixture analysis, *Remote Sensing of Environment*, 59:472–489.

Van der Meer, F., 1999. Iterative spectral unmixing (ISU), *International Journal of Remote Sensing*, 20:3431–3436.

Vieira, I.C.G., A.S. de Almeida, E.A. Davidson, T.A. Stone, C.J.R. de Carvalho, and J.B. Guerrero, 2003. Classifying successional forests using Landsat spectral properties and ecological characteristics in eastern Amazonia, *Remote Sensing of Environment*, 87:470–481.

(Received 27 February 2004; accepted 14 April 2004; revised 28 May 2004)